

Cite this: *Phys. Chem. Chem. Phys.*, 2011, **13**, 9008–9013

www.rsc.org/pccp

PAPER

## Novel ice structures in carbon nanopores: pressure enhancement effect of confinement

Monika Jazdzewska,<sup>a</sup> Małgorzata M. Śliwiska-Bartkowiak,<sup>a</sup> Anatoly I. Beskrovnyy,<sup>bc</sup> Sergey G. Vasilovskiy,<sup>b</sup> Siu-Wa Ting,<sup>d</sup> Kwong-Yu Chan,<sup>d</sup> Liangliang Huang<sup>e</sup> and Keith E. Gubbins<sup>\*e</sup>

Received 6th December 2010, Accepted 8th March 2011

DOI: 10.1039/c0cp02797a

We report experimental results on the structure and melting behavior of ice confined in multi-walled carbon nanotubes and ordered mesoporous carbon CMK-3, which is the carbon replica of a SBA-15 silica template. The silica template has cylindrical mesopores with micropores connecting the walls of neighboring mesopores. The structure of the carbon replica material CMK-3 consists of carbon rods connected by smaller side-branches, with quasi-cylindrical mesopores of average pore size 4.9 nm and micropores of 0.6 nm. Neutron diffraction and differential scanning calorimetry have been used to determine the structure of the confined ice and the solid–liquid transition temperature. The results are compared with the behavior of water in multi-walled carbon nanotubes of inner diameters of 2.4 nm and 4 nm studied by the same methods. For D<sub>2</sub>O in CMK-3 we find evidence of the existence of nanocrystals of cubic ice and ice IX; the diffraction results also suggest the presence of ice VIII, although this is less conclusive. We find evidence of cubic ice in the case of the carbon nanotubes. For bulk water these crystal forms only occur at temperatures below 170 K in the case of cubic ice, and at pressures of hundreds or thousands of MPa in the case of ice VIII and IX. These phases appear to be stabilized by the confinement.

### 1. Introduction

Water confined in a nanoscale environment exhibits unique properties and has been the subject of much attention. Of particular interest have been the effects of confinement on phase transitions, on the structure of water and ice in nanopores,<sup>1–3</sup> and on dynamical properties of water in one-dimensional pores considered as a model of water channels.<sup>4,5</sup>

There are at least 16 ice polymorphs of bulk water. The phase diagram of ice exhibits many different crystal forms, depending on local molecular correlations that influence the ordered arrangement of hydrogen-bonded configurations. Some of these forms are found only at pressures above 100 MPa (*e.g.* ice VII, VIII, IX, X and XI) and/or at temperatures below about 170 K (*e.g.* ice Ic, IX, XI), while some (*e.g.* cubic ice Ic) are metastable in the bulk.

Much less is known about the phase behavior of confined water. It is frequently observed that phase changes that only occur at high pressures or low temperatures in the bulk phase occur in the confined phase at pressures that are orders of magnitude lower (bulk phase pressure in equilibrium with the confined phase) and at normal temperatures.<sup>6,7</sup> A familiar example is vapor–liquid condensation in the confined phase (capillary condensation), but similar phenomena are observed for solid phases. The structure of confined ice has been studied in carbon nanotubes of diameters 0.7–1.5 nm using molecular simulations<sup>8–10</sup> and experiments,<sup>11</sup> and provides convincing evidence for the formation of different kinds of ice nanocrystals, identified as polygonal ice in nanotubes of small diameters, including square ice nanotube, a further example of the quasi-high pressure effect in confinement. Similar quasi-high pressure effects due to confinement are observed in chemical reactions in pores. Reactions that only occur at high pressures in the bulk phase occur readily at normal bulk phase pressures in the confined phase, as has been observed in experiments<sup>12</sup> and molecular simulations.<sup>13</sup> The origin of these quasi-high pressure effects on confinement has been shown to be due to the strong intermolecular forces between the walls of the pores and the molecules of the confined phase (capillary forces, in macroscopic parlance), leading to effective pressure

<sup>a</sup> Faculty of Physics, A. Mickiewicz University, Poznan, Poland 61614

<sup>b</sup> Frank Laboratory of Neutron Physics, Joint Institute for Nuclear Research, Dubna, Russia 141980

<sup>c</sup> Russian Research Centre Kurchatov Institute, Moscow, Russia, 123182

<sup>d</sup> Department of Chemistry, University of Hong Kong, Pokfulam Road, Hong Kong

<sup>e</sup> Department of Chemical and Biomolecular Engineering, North Carolina State University, Raleigh, NC, 27695, USA. E-mail: keg@ncsu.edu

in the pores that are orders of magnitude higher than in the bulk phase.<sup>14,15</sup>

Recent studies for pores of simple geometry have shown a rich phase behavior associated with melting in confined systems.<sup>7,16</sup> The melting temperature may be lowered or raised relative to the bulk melting temperature, depending on the nature of the adsorbate and the porous material. Much of the apparently complex phase behavior is a result of competition between the fluid-wall and fluid-fluid intermolecular interactions. For water confined in carbons a decrease in the melting point relative to bulk water was observed due to the small ratio of fluid-wall/liquid-liquid attractive interaction.<sup>17,18</sup>

In this paper we report experimental studies of the melting transition for D<sub>2</sub>O water confined in CMK-3 porous carbon and in multi-walled carbon nanotubes of similar inner diameters.

## 2. Methods

The CMK-3 was synthesized according to the literature procedure<sup>19</sup> using furfuryl alcohol as carbon precursor. A SBA-15 mesoporous silica template was synthesized according to Zhao *et al.*<sup>20</sup> We performed nitrogen sorption experiments on a Micromeritics ASAP 2020 porosimetry analyzer. The desorption branch of the isotherm was analyzed using the density functional theory (DFT) method to yield pore size distributions (psd) as shown in Fig. 1. A major peak at 4.9 nm is shown in the DFT psd, with a second peak showing micropores of 0.6 nm, assuming cylindrical pores. For comparison, the water melting behavior in quasi-cylindrical carbon pores in opened multi-walled carbon nanotubes (MWNT) having average inner diameters of 2.4 nm and 4.0 nm, produced by NANOCYL Belgium, was studied using differential scanning calorimetry (DSC). The structure of the confined ice was determined by neutron diffraction. D<sub>2</sub>O water was used in the neutron scattering study to avoid the complications of incoherent scattering and inelasticity corrections that arise when H<sub>2</sub>O is used.

Porous carbon samples were heated to about 400 K and kept under vacuum ( $10^{-3}$  torr) for several days to remove air prior to and during the introduction of D<sub>2</sub>O (100% deuterium purchased from Sigma) or H<sub>2</sub>O water. The H<sub>2</sub>O water samples were distilled and demineralised using a Millipore apparatus. The conductivity of the purified water was on the order of  $10^{-4} \Omega^{-1} \text{ m}^{-1}$ .

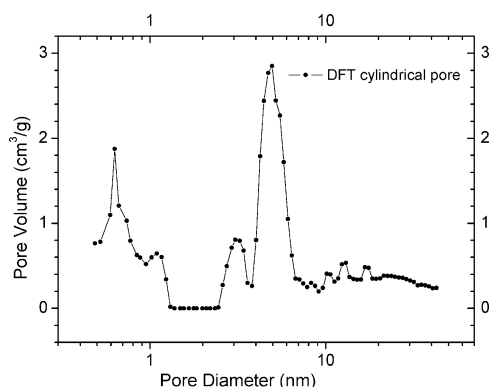


Fig. 1 Pore size distribution (DFT) for CMK-3.

## Differential scanning calorimetry

A Netzsch DSC204 Phoenix differential scanning calorimeter (DSC) was used to determine the melting temperatures of the bulk and confined water by measuring the heat released on the melting of H<sub>2</sub>O and D<sub>2</sub>O. The temperature scanning rates were 2–5 K min<sup>-1</sup>. The melting temperatures were determined from the position of the peaks of the heat flow signals on heating and were reproducible to within 0.5 K.

## Neutron diffraction

The crystal structure of the ice was investigated by neutron powder diffraction performed in the high luminosity DN-2 time-of-flight powder diffractometer at the Frank Laboratory of Neutron Physics of the Joint Institute for Nuclear Dubna Research (JINR) with the fast pulsed reactor IBR-2 (<http://flnp.jinr.ru/137/>). The resolution of the diffraction patterns was determined by the width of the pulse from the neutron source,  $\Delta d/d = 0.01$ , in the range of interplanar spacings  $d_{hkl}$  from 1 to 20 Å. The scattering angle  $2\theta \approx 176^\circ$  was fixed. The sample was placed in a vanadium container of diameter 5 mm, height 15 mm, and was cooled to about 20 K and then warmed to 300 K. Structure refinement was carried out using the FullProf program, based on the multi-phase Rietveld analysis method.<sup>21–23</sup> This structure refinement method, which does not use integrated neutron powder intensities, single or overlapping, employs the profile intensities obtained from step-scanning measurements of the powder diagram. The nuclear structure can be refined with the assumption of the Gaussian peak shape for each Bragg peak.

## 3. Experimental results

The melting temperature of water confined in CMK-3 and in MWNT's with inner diameters of 2.4 and 4 nm was determined using the DSC method. The measurements were performed for both H<sub>2</sub>O and D<sub>2</sub>O water, as D<sub>2</sub>O is used in the neutron scattering experiments. The DSC scans corresponding to the melting of H<sub>2</sub>O and D<sub>2</sub>O water in CMK-3, and of H<sub>2</sub>O in MWNT's are presented in Fig. 2a, b and 3a, b respectively.

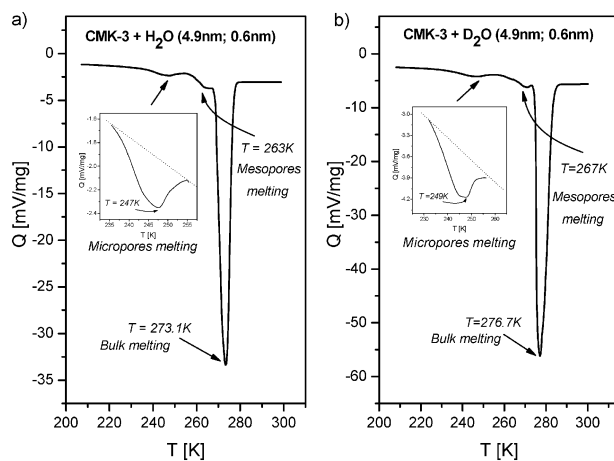
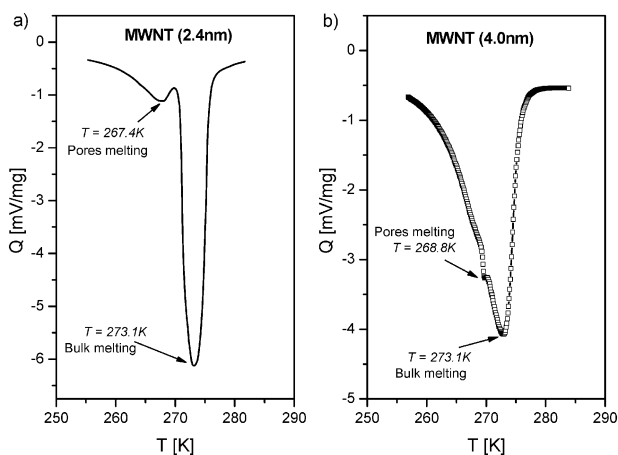


Fig. 2 DSC scan ( $5 \text{ K min}^{-1}$ ) for: (a) H<sub>2</sub>O confined in CMK-3, with mesopores ( $D = 4.9 \text{ nm}$ ) connected by micropores ( $D' = 0.6 \text{ nm}$ ); (b) D<sub>2</sub>O confined in CMK-3.



**Fig. 3** DSC scan ( $5 \text{ K min}^{-1}$ ) for: (a)  $\text{H}_2\text{O}$  confined in multi-walled carbon nanotubes with diameter  $D = 2.4 \text{ nm}$ ; (b)  $\text{H}_2\text{O}$  confined in MWNT with diameter  $D = 4.0 \text{ nm}$ .

The large endothermic peak at  $273.1 \text{ K}$  shown in Fig. 2a corresponds to the melting of the bulk  $\text{H}_2\text{O}$  water in which the porous carbons are suspended, so the pores are fully filled. In Fig. 2a the endothermic peaks observed at temperatures  $263 \text{ K}$  and  $247 \text{ K}$  can be attributed to the melting of water in the CMK-3 mesopores of diameter  $4.9 \text{ nm}$  and micropores of diameter  $0.6 \text{ nm}$ , respectively. A DSC scan, corresponding to the melting of  $\text{D}_2\text{O}$  water in CMK-3, is presented in Fig. 2b. The large endothermic peak at  $276.7 \text{ K}$  corresponds to the melting of the bulk  $\text{D}_2\text{O}$ ; the peaks at temperatures  $267 \text{ K}$  and  $249 \text{ K}$  indicate the melting points in mesopores and micropores respectively. The shift of the melting temperatures towards lower temperatures for  $\text{H}_2\text{O}$  in mesopores of CMK-3 relative to bulk water,  $\Delta T = T_{\text{pore}} - T_{\text{bulk}}$ , is about  $10 \text{ K}$  (for  $\text{D}_2\text{O}$  it is  $9.7 \text{ K}$ ) and for  $\text{H}_2\text{O}$  and  $\text{D}_2\text{O}$  in micropores of CMK-3 it is:  $\Delta T = 26 \text{ K}$  and  $\Delta T = 27.7 \text{ K}$  respectively. In Fig. 3a and b peaks at  $267.4 \text{ K}$  and  $268.8 \text{ K}$  are observed, and are believed to correspond to the melting of  $\text{H}_2\text{O}$  water in the MWNT's of diameters  $2.4 \text{ nm}$  and  $4 \text{ nm}$ , respectively. We conclude that the melting temperature of  $\text{H}_2\text{O}$  adsorbed in MWNT's is shifted towards lower temperatures by about  $5.7 \text{ K}$  for MWNT's of  $2.4 \text{ nm}$  in diameter and by  $4.3 \text{ K}$  for MWNT's of  $4 \text{ nm}$  in diameter relative to that of bulk water. Similar shifts of pore melting temperatures were observed for  $\text{D}_2\text{O}$  in MWNT's of the same diameters.<sup>24</sup>

In order to characterize the structure of water confined in carbon meso- and micropores we performed neutron diffraction studies for  $\text{D}_2\text{O}$  water in CMK-3 and MWNT's of similar inner diameters. The neutron diffraction pattern and the Rietveld refinement for the CMK-3 and MWNT of diameters  $2.4$  and  $4 \text{ nm}$  of powder samples are shown in Fig. 4 at  $293 \text{ K}$ . The graphite 3D crystal has a hexagonal structure (space group  $P63/mmc$ ). Neutron diffraction revealed the (110), (101) and (002) reflections of the hexagonal lattice of the dry CMK-3 and also MWNT. In common with most purified carbon materials our samples contain impurities and exhibit local defects (holes, cross-links).<sup>25</sup> The local defects and varying microstructure do not affect the interpretation of the neutron data regarding the encapsulated  $\text{D}_2\text{O}$  water, because the low impurity concentration and much larger length scale of

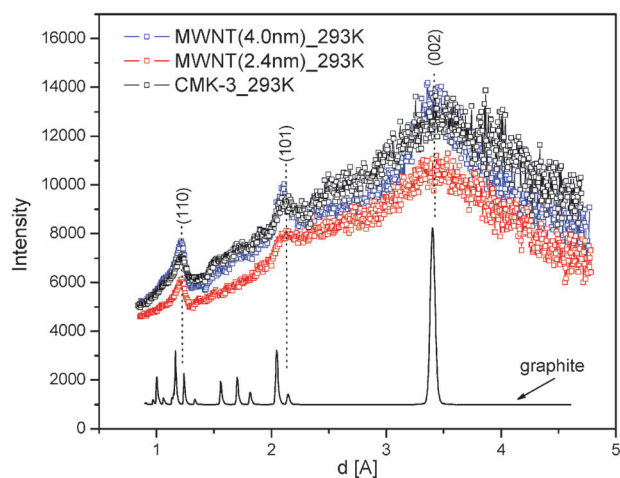


**Fig. 4** Neutron diffraction pattern and the results of the Rietveld refinement of empty MWNT's of  $2.4 \text{ nm}$  and  $4.0 \text{ nm}$  diameters and CMK-3 at temperatures of  $293 \text{ K}$ .

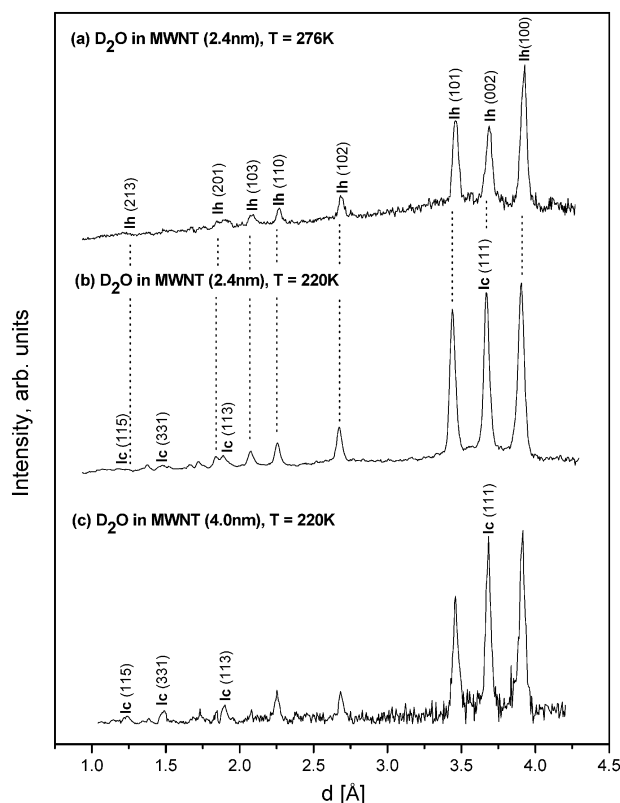


**Fig. 5** The diffraction pattern for  $\text{D}_2\text{O}$  in: (a) MWNT,  $D = 2.4 \text{ nm}$  at  $T = 276 \text{ K}$ ; (b) MWNT,  $D = 2.4 \text{ nm}$  at  $T = 220 \text{ K}$ ; (c) MWNT,  $D = 4.0 \text{ nm}$  at  $T = 220 \text{ K}$ .

the microstructure defects compared to the  $\text{D}_2\text{O}$  water molecules only lead to a negligible and featureless background in the neutron intensity. In Fig. 5 we present the neutron diffraction patterns for  $\text{D}_2\text{O}$  water encapsulated in MWNT of diameter  $2.4 \text{ nm}$  at temperatures  $276 \text{ K}$  (a) and  $220 \text{ K}$  (b) and MWNT of diameter  $4 \text{ nm}$  at temperature  $220 \text{ K}$  (c) obtained during a warming cycle after Rietveld refinements. At  $276 \text{ K}$ , slightly below the bulk  $\text{D}_2\text{O}$  water melting point but higher

than the pore melting temperature, the neutron diffraction spectrum is typical for hexagonal ice (Ih) with the space group  $P63/mmc$ , and represents the ice in the bulk phase. The characteristic triplet of hexagonal ice is clearly visible at 3.44, 3.66 and 3.89 Å, with additional single peaks at the positions 1.26, 1.88, 2.25 and 2.67 Å. A similar neutron diffraction spectrum was observed for D<sub>2</sub>O encapsulated in MWNT's of 4 nm in diameter at the temperature 275 K. The neutron diffraction patterns for D<sub>2</sub>O in MWNT's of diameters 2.4 and 4 nm are shown in Fig. 5b and c at temperature 220 K. At this lower temperature, below the pore melting point, there is a broader peak, structure characteristic of cubic ice (Ic) with the space group  $Fd3m$ , where additional peaks at positions 1.22, 1.46, 1.91 and 3.67 Å are observed. The Rietveld refinement of diffraction patterns in the region of the main peaks ( $\sim 3.4$  to 4.0 Å) is shown in Fig. 6. The changes of the spectrum as a function of temperature for D<sub>2</sub>O in MWNT's of 2.4 nm in diameter are shown in Fig. 6a and b. The sequence illustrates the difference between the composite phase where hexagonal ice has formed outside the pores but there is still liquid in the pores (Fig. 6a), and the phase is showing the characteristic triplet shape of a form of cubic ice at  $d = 3.65$ –3.69 Å (Fig. 6b). The hexagonal ice peaks are sharp,

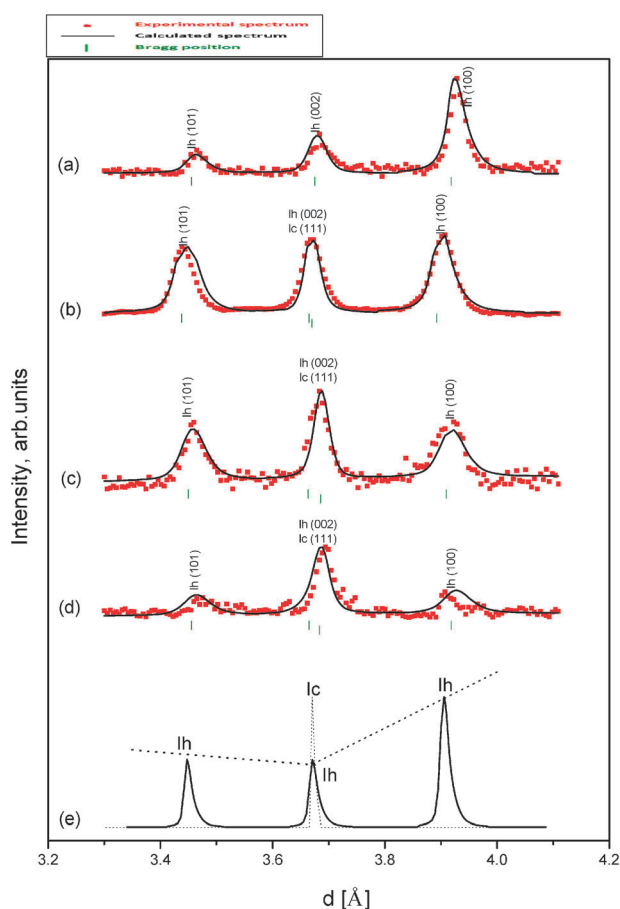


**Fig. 6** Rietveld refinement of the diffraction pattern for D<sub>2</sub>O; (a) MWNT,  $D = 2.4$  nm,  $T = 276$  K; (b) MWNT,  $D = 2.4$  nm,  $T = 220$  K; (c) MWNT,  $D = 4.0$  nm,  $T = 220$  K; (d) CMK-3,  $D = 4.9$  nm,  $T = 240$  K; (e) Rietveld refinements of the diffraction pattern for Ih and Ic.

indicating a large crystallite size, and the peak positions show a systematic displacement with temperature. The results of the Rietveld refinement for the diffraction pattern of Ih and Ic ice presented in Fig. 6e show that the spectrum obtained at temperature 220 K (Fig. 6b) is a superposition of the Ih and Ic spectrum. In Fig. 6c and d the neutron diffraction patterns for D<sub>2</sub>O in MWNT's of diameter 4 nm at 220 K (Fig. 6c) and for D<sub>2</sub>O in CMK-3 at 240 K (Fig. 6d) are presented. These results show the existence of ice in the bulk phase D<sub>2</sub>O and the characteristic triplet shape of cubic ice Ic at 3.65–3.68 Å, attributed to ice in the mesopores, at temperatures below the pore melting point for both MWNT's and CMK-3.

In Fig. 7a the complete neutron diffraction pattern observed for D<sub>2</sub>O in CMK-3 at 240 K recorded on a heating cycle is presented. The peaks observed at the positions 3.91 Å (111), 3.02 Å (201), 2.25 Å (212), 2.04 Å (311) and 1.87 Å (320) are characteristic of the crystal space group ( $P4(1)2(1)2$ )—the form of ice IX, while the peaks at positions 2.38 Å (112), 1.65 Å (220) and 1.38 Å (204) are characteristic of the space group ( $I4(1)/amd$ ), corresponding to ice VIII. At the positions 3.65–3.68 Å the characteristic triplet shape showing the existence of cubic ice Ic and hexagonal ice Ih is observed. At a temperature of 290 K, D<sub>2</sub>O bulk and D<sub>2</sub>O inside the pores are in the liquid phase and in the neutron diffraction pattern only the peaks from CMK-3 are visible (Fig. 7b).

The theoretical estimation of the diffraction pattern of Ih ( $P63/mmc$  space group), Ic ( $Fd3m$ ), ice IX ( $P4(1)2(1)2$ ) and ice VIII ( $I4(1)/amd$ ) separately obtained on the basis of the data from the Crystallographic and Crystallochemical Database for Minerals and their Structural Analogues<sup>26</sup> is presented in Fig. 8. The results of the Rietveld refinement for the diffraction pattern of Ih, Ic, VIII and IX shown in Fig. 8 are presented in Fig. 9 with comparison of the diffractogram observed for D<sub>2</sub>O in CMK-3 at 240 K. It confirms that the experimentally obtained diffractogram contains these four kinds of ice spectra. The formation of ice IX and ice VIII in CMK-3 at 240 K, somewhat below the freezing temperature for the micropores, could be due to structures of ice in either the mesopores or the 0.6 nm micropores of CMK-3. We note that

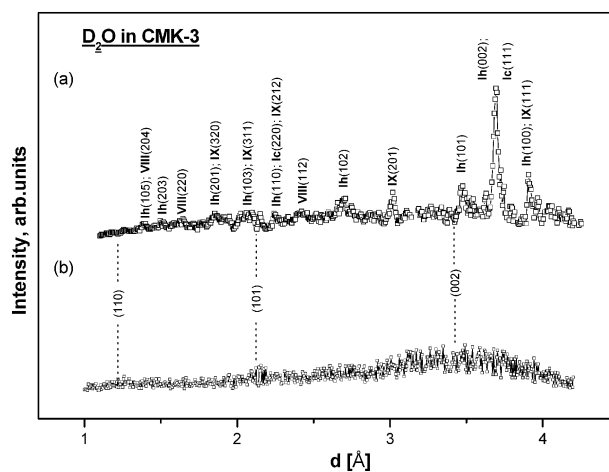


**Fig. 7** Neutron diffraction pattern for D<sub>2</sub>O in CMK-3 porous carbon: (a)  $T = 240$  K; (b)  $T = 290$  K.

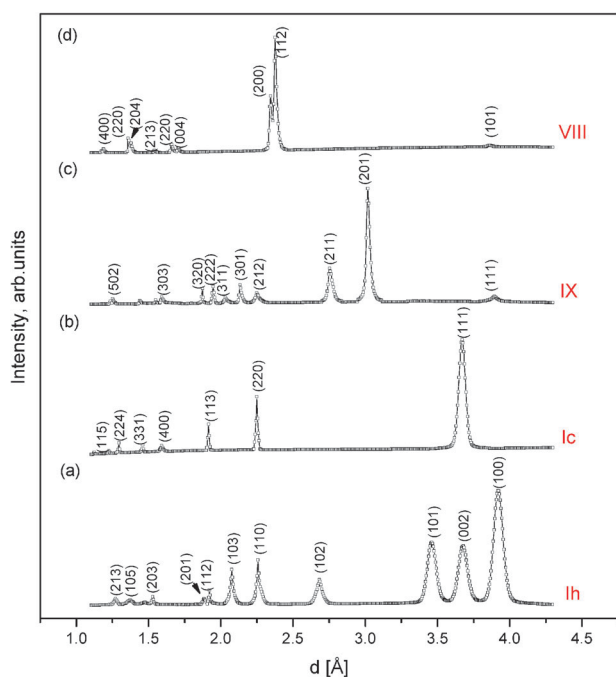


**Fig. 8** The diffraction pattern of the crystal structure of ice forms: (a) hexagonal ice; (b) cubic ice; (c) ice IX; (d) ice VIII.

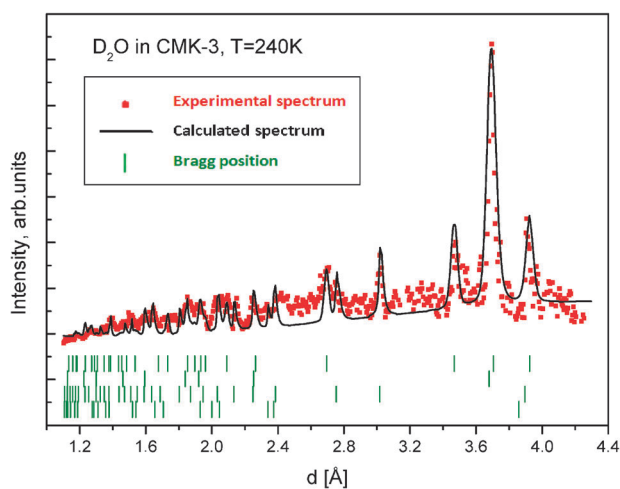


**Fig. 9** Neutron diffraction pattern and the result of the Rietveld refinement of  $D_2O$  in CMK-3 at  $T = 240$  K.

the formation of tetragonal, ordered ice (the form of ice IX and ice VIII) in carbon nanotubes having diameters of 0.7–1.5 nm, slightly larger than the micropores in CMK-3, was postulated theoretically<sup>8–10</sup> for nanotubes of about 1 nm in diameter.

#### 4. Discussion

Our results provide strong evidence for the presence of ice Ic in both carbon nanotubes at 220 K and in CMK-3 at 240 K. This phase is metastable and is only observed at temperatures below about 170 K in bulk water, but is apparently stabilized in the confined phase. This provides an example of the quasi-low temperature effect due to confinement in carbon

materials.<sup>6,7</sup> We also find evidence of the formation of tetragonal forms of ice in CMK-3 at temperatures below the pore melting point, with peaks corresponding to nanocrystals of ice IX, and suggestive of ice VIII. Molecular simulation results<sup>8–10</sup> for water confined in carbon nanotubes have predicted similar ice forms for nanotubes of diameters below 1 nm. While we cannot determine whether these tetragonal forms of ice are occurring in the mesopores or micropores from our observations alone, the simulation results suggest the latter. Ice VIII and ice IX occur only at pressures of  $\sim 1$  GPa and above in bulk water. Their presence in CMK-3 at 240 K provides an example of the quasi-high pressure effect under confinement.<sup>7</sup> The range of the depression of the melting temperature observed for  $H_2O$  in meso- and micropores of CMK-3 is comparable with that for  $H_2O$  confined in carbon nanotubes of similar diameters.<sup>9,24</sup>

#### Acknowledgements

This work was supported by a grant from the Polish Ministry of Higher Education and Informatics, Nr. N 202 07 03 33. KEG and LLH thank the U.S. National Science Foundation for partial support of this work (grant no. CBET-0932656). KYC thanks the support of HK RGC (Grant HKU 700209P). Helpful discussion with Dr M. Thommes, Quantachrome Instruments, on interpretation of pore size distribution was most appreciated.

#### References

- 1 A. Striolo, A. A. Chialvo, K. E. Gubbins and P. T. Cummings, *J. Chem. Phys.*, 2005, **122**, 234712.
- 2 A. I. Kolesnikov, J. M. Zanotti, C. K. Lonng, P. Thiyagarajan, A. P. Moravsky, R. O. Loufty and C. J. Burnham, *Phys. Rev. Lett.*, 1999, **93**, 035503.
- 3 H. Tanaka and K. Koga, *J. Chem. Phys.*, 2005, **123**, 094706.
- 4 J. C. Dore, B. Webber and J. H. Strange, *Colloids Surf., A*, 2004, **241**, 191.
- 5 K. Matsuda, T. Hibi, H. Kadouaki, H. Kataura and Y. Maniwa, *Phys. Rev. B: Condens. Matter Mater. Phys.*, 2006, **74**, 073415.
- 6 L. D. Gelb, K. E. Gubbins, R. Radhakrishnan and M. Sliwinski-Bartkowiak, *Rep. Prog. Phys.*, 1999, **62**, 1573.
- 7 C. Alba-Simonesco, B. Coasne, G. Dudziak, K. E. Gubbins, R. Radhakrishnan and M. Sliwinski-Bartkowiak, *J. Phys.: Condens. Matter*, 2006, **18**, R14.
- 8 K. Koga, G. T. Gao, H. Tanaka and X. C. Zeng, *Nature*, 2001, **412**, 802.
- 9 J. Bai, J. Wang and X. C. Zeng, *Proc. Natl. Acad. Sci. U. S. A.*, 2006, **183**, 19664.
- 10 D. Takaiwa, I. Hatano, K. Koga and H. Tanaka, *Proc. Natl. Acad. Sci. U. S. A.*, 2008, **105**, 39.
- 11 Y. Maniwa, H. Kataura, M. Abe, A. Udaka, S. Suzuki, Y. Achiba, H. Kira, K. Matsuda, H. Kadowaki and Y. Okabe, *Chem. Phys. Lett.*, 2005, **401**, 534.
- 12 For example: K. Kaneko, N. Fukuzaki, K. Kakei, T. Suzuki and S. Ozeki, *Langmuir*, 1989, **5**, 960; J. Imai, M. Souma, S. Ozeki, T. Suzuki and K. Kaneko, *J. Phys. Chem.*, 1991, **95**, 9955; Y. Nishi, T. Suzuki and K. Kaneko, *J. Phys. Chem. B*, 1997, **101**, 1938; T. Yamamoto, D. A. Tryk, K. Hashimoto, A. Fujishima and M. Okawa, *J. Electrochem. Soc.*, 2000, **147**, 3393; O. Byl, P. Kondratyuk and J. T. Yates Jr., *J. Phys. Chem. B*, 2003, **107**, 4277.
- 13 C. H. Turner, J. K. Johnson and K. E. Gubbins, *J. Chem. Phys.*, 2001, **114**, 1851.
- 14 M. Miyahara, H. Kanda, M. Shibao and K. Higashitani, *J. Chem. Phys.*, 2000, **112**, 9909.

- 15 B. Coasne, J. Czwartos, M. Śliwinska-Bartkowiak and K. E. Gubbins, *J. Phys. Chem. B*, 2009, **113**, 13874.
- 16 K. Koga, G. T. Gao, H. Tanaka and X. C. Zeng, *Nature*, 2001, **412**, 802.
- 17 M. Sliwinska-Bartkowiak, G. Dudziak, R. Sikorski, R. Gras, R. Radhakrishnan and K. E. Gubbins, *J. Chem. Phys.*, 2001, **114**, 950.
- 18 R. Radhakrishnan, K. E. Gubbins and M. Sliwinska-Bartkowiak, *J. Chem. Phys.*, 2002, **116**, 1147.
- 19 R. Ryoo, S. H. Joo and S. Jun, *J. Phys. Chem. B*, 1999, **103**, 7743.
- 20 D. Y. Zhao, J. L. Feng and Q. S. Huo, *Science*, 1998, **297**, 548.
- 21 A. Beskrovny, N. Guskos, J. Typek, N. Ryabova, A. Blonska-Tabero and G. Zolnierkiewicz, *Rev. Adv. Mater. Sci.*, 2006, **12**, 166.
- 22 H. M. Rietveld, *J. Appl. Crystallogr.*, 1969, **2**, 65.
- 23 V. B. Zlokazov and V. V. Chernyshev, *J. Appl. Crystallogr.*, 1992, **25**, 447.
- 24 M. Sliwinska-Bartkowiak, M. Jazdzewska, L. L. Huang and K. E. Gubbins, *Phys. Chem. Chem. Phys.*, 2008, **10**, 4957.
- 25 M. Bazarnik, M. Cegiel, P. Biskupski, M. Jazdzewska, S. Mielcarek, M. Śliwinska-Bartkowiak and R. Czajka, *Cent. Eur. J. Phys.*, 2009, **7**(2), 295–298.
- 26 <http://database.iem.ac.ru/mincryst/>.